

Intrinsic unpredictability of strong El Niño events

John Guckenheimer and Andrew Roberts

*Mathematics Department, Cornell University, Ithaca, NY 14853**

Axel Timmermann

*International Pacific Research Center, School of Ocean and Earth Science and Technology,
University of Hawaii at Manoa, Honolulu, Hawaii, 96822*

Henk Dijkstra

*Institute for Marine and Atmospheric research Utrecht,
Department of Physics and Astronomy, Utrecht University, Utrecht, The Netherlands*

(Dated: July 12, 2016)

The El Niño-Southern Oscillation (ENSO) is a mode of interannual variability in the coupled equatorial ocean/atmosphere Pacific. El Niño describes a state in which sea surface temperatures in the eastern Pacific increase and upwelling of colder, deep waters diminishes. El Niño events typically peak in boreal winter, but their strength varies irregularly on decadal time scales. There were exceptionally strong El Niño events in 1982-83, 1997-98 and 2015-16 that affected weather on a global scale. Widely publicized forecasts in 2014 predicted that the 2015-16 event would occur a year earlier. Predicting the strength of El Niño is a matter of practical concern due to its effects on hydroclimate and agriculture around the world. This paper presents a new robust mechanism limiting the predictability of strong ENSO events: the existence of an irregular switching between an oscillatory state that has strong El Niño events and a chaotic state that lacks strong events, which can be induced by very weak seasonal forcing or noise.

The problem in predicting El Niño events is that they occur quite irregularly, and their development seems to be different each time [1]. The ENSO phenomenon is thought to be an internal mode of the coupled equatorial ocean-atmosphere system which can be self-sustained or excited by random noise [2]. The interactions of the internal mode and the external seasonal forcing can lead to chaotic behavior through nonlinear resonances [3, 4]. On the other hand, the dynamical behavior can be strongly influenced by noise, in particular westerly wind bursts [5] which can either be viewed as additive [6] or multiplicative noise [7]. During boreal spring the coupled ocean-atmosphere system is thought to be at its frailest state [8]. Then the system is most susceptible to perturbations [9] which leads to a ‘spring’ predictability barrier in April/May [10]. The role of the initial error pattern has been emphasized and in particular its interaction with the seasonal cycle and the internal cycle [11–13].

Processes determining ENSO variability and its limits of predictability have been discovered with conceptual models [14–16]. Such models seek to identify key dynamical processes in the complex, coupled atmosphere/ocean system in the tropical Pacific. This paper investigates the predictability of El Niño using the low-dimensional conceptual Jin-Timmermann (JT) model of ENSO originally proposed by Jin [16] and then extended by Timmermann et al. [17]. The state space variables of this deterministic model are sea surface temperatures of the equatorial western Pacific and eastern Pacific, and the thermo-

cline depth (e.g. the depth of the 20°C isotherm) of the Western Pacific. Nonlinear terms in the model represent feedbacks due to winds, ocean currents and thermocline dynamics that affect these state variables. Comparisons of this reduced order model with simulations of coupled global climate models confirm that the model embodies the basic features of ENSO in the tropical Pacific [18].

Recently, a multiple time scale analysis of the JT model was performed to gain new insight into the dynamics [19]. This work transformed the model equations into an equivalent dimensionless system whose equations are

$$\begin{cases} x' &= \rho\delta(x^2 - ax) + x(x + y + c - c \tanh(x + z)) \\ y' &= -\rho\delta(ay + x^2) \\ z' &= \delta(k - z - \frac{x}{2}), \end{cases} \quad (1)$$

The variables x , y and z of this model represent the sea surface temperature difference between the eastern and western equatorial Pacific, sea surface temperature of the western equatorial Pacific relative to a nominal reference temperature, and thermocline depth of the western Pacific, respectively. Each of the five parameters δ , ρ , c , k and a represents a combination of physical characteristics of the tropical Pacific. Time dependent effects from the climatological annual cycle of the air-sea heat flux [20] will be included to the model as explored below.

This paper focuses attention on the behavior of the model with parameters

$$[\delta, \rho, c, k, a] = [0.225423, 0.3224, 2.3952, 0.4032, 7.3939]$$

where there is bistability between a periodic orbit and a chaotic attractor. The green trajectory in Figure (1)

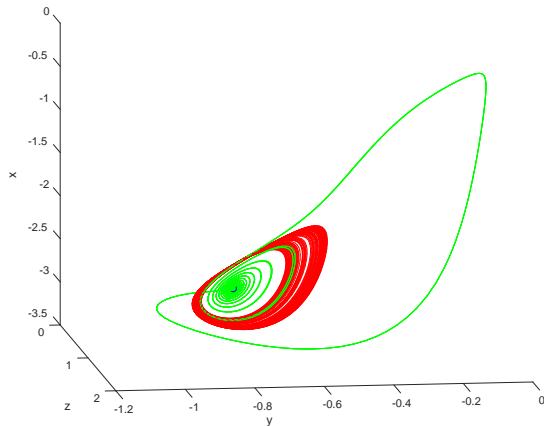


FIG. 1. Phase portrait of a chaotic attractor (red) and an MMO periodic orbit (green) that coexist at parameters $[\delta, \rho, c, k, a] = [0.225423, 0.3224, 2.3952, 0.4032, 7.3939]$. The equilibrium point is a partially obscured blue dot.

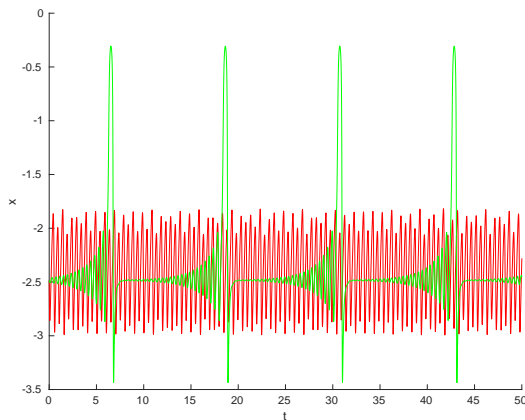


FIG. 2. Time series of the x coordinate of the two trajectories shown in Figure (1). Units of time are years.

is a mixed mode oscillation (MMO) with period approximately 12.1 years and a single intense El Niño event each period, which emerges after a series of growing interannual oscillations. The red trajectory is chaotic but the amplitude of its oscillations varies in a much narrower range than those of the MMO.

A central feature of the MMO cycle is an equilibrium point that is a saddle focus: the MMO approaches the equilibrium along its one dimensional stable manifold and then spirals away, following the two dimensional unstable manifold of the equilibrium. The number of oscillations of the MMO cycle and their minimum amplitude depends upon how close it approaches the equilibrium. The growing amplitude oscillations of the MMO cycle terminate in an intense El Niño where the sea surface temperatures of eastern and western tropical Pacific are almost the same.

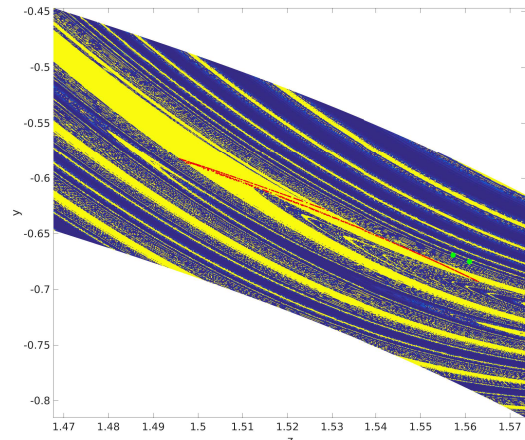


FIG. 3. The colored region is a 500x500 grid that straddles the intersection of the chaotic attractor with the cross-section $x = -2.874$. Points are colored by whether the trajectories originating from the points approach the chaotic attractor (yellow) or the MMO (blue). The red markers and green dots mark intersections of the chaotic attractor and MMO with the cross-section, respectively

This El Niño is followed by a La Niña event in which the system “recharges” [16], reestablishing higher sea surface temperatures and thermocline depth in the western than eastern Pacific. The recharged system flows back toward the equilibrium where the cycle repeats.

The chaotic attractor is similar to those found in many other three dimensional vector fields. It can be analyzed by introducing a cross-section and studying its discrete time return map. The return map contracts a strip in one direction, and stretches and folds in the second direction. There is sensitivity to initial conditions within the chaotic attractor, but it is relatively mild: nearby initial conditions separate along the attractor without leaving it.

The basins of attraction of the two attractors are intertwined with each other in an intricate way. They display fractal basin boundaries [21]. Even though almost all initial conditions presumably approach one of the two attractors, there are large regions in which it is difficult to predict which basin a chosen initial condition will belong to (Figure (3)). Note that both attractors are very close to their basin boundaries. This suggests that there are nearby trajectories that separate abruptly. This is displayed in Figure (4) which plots the third return of the y coordinate in a strip of width 0.035 which spans points that lie in the basin of attraction of the MMO. The plateau of this map consists of points that make a large amplitude oscillation and tend to the MMO attractor. On either side of the basin, the relative distances between points of the steep region are expanded by the return map by as much as 10^3 : there is very high sensitiv-

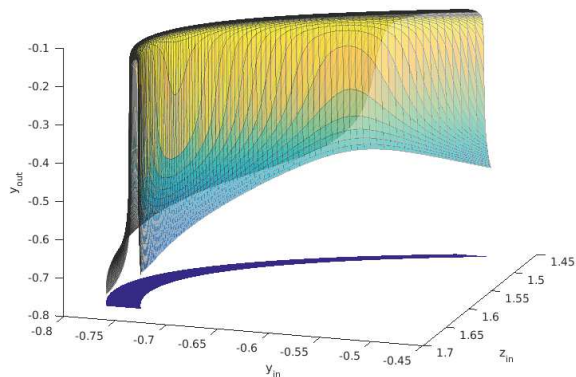


FIG. 4. The image of the y -coordinate under the third iterate of the return map of a thin strip of initial conditions (dark blue) of width 0.035 in the cross section. Points in the middle of the strip make a large amplitude excursion representing a strong El Niño. The map stretches the y -coordinate by a factor of order 10^3 where the returns have intermediate amplitude.

ity to initial conditions here. This prompts the question as to whether small modifications of the system cause switching between the two attractors by creating trajectories that visit the plateau of this (third) return map on some returns but not other.

To investigate switching between the attractors, the model was modified by making the parameter a a sinusoidal function of time with a period of one year to mimic effects of the annual solar cycle [17, 20]. Figure (5) shows the results of setting the amplitude of the periodic forcing to 0.001. Even at this small forcing amplitude, the system switches erratically between its two modes of variability. In a longer simulation of 6000 years, the largest number of consecutive MMO cycles was 24 and the smallest number was 1. Some epochs of chaotic oscillations were over 200 years in duration. There is no apparent pattern to these durations, so it seems that the timing of strong El Niño events is unpredictable on a decadal time cycle. No attempt was made to identify precursors to these events, but that is clearly a matter of practical interest. Similar results can be obtained by including weak multiplicative forcing of the parameter a instead of periodic forcing as shown in Figure (6).

Reconstructions of past climate from historical data indicate that ENSO is highly variable with long periods of larger and smaller variance on decadal time scales [22, 23]. The above results demonstrate the existence of a new mechanism limiting predictability of strong ENSO events. This extreme variability appears in a simple low-dimensional model that incorporates coupling of basin-wide atmospheric and oceanic waves and adjustment. Rapid divergence of nearby trajectories from

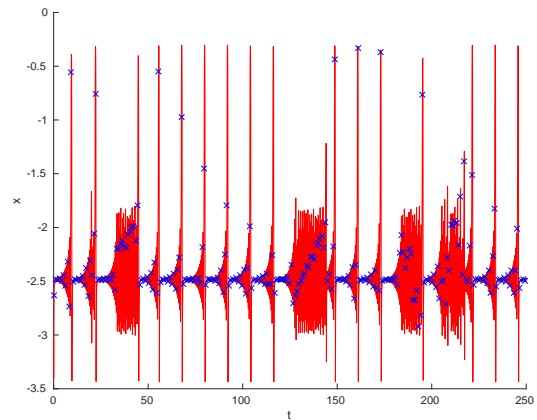


FIG. 5. Time series for the x coordinate of the model with the parameter a modified to be the periodic function of time $a = 7.3939 + 0.001 \sin(1.8t)$. The frequency and the units of time are years. The crosses are points at a specific phase of the forcing.

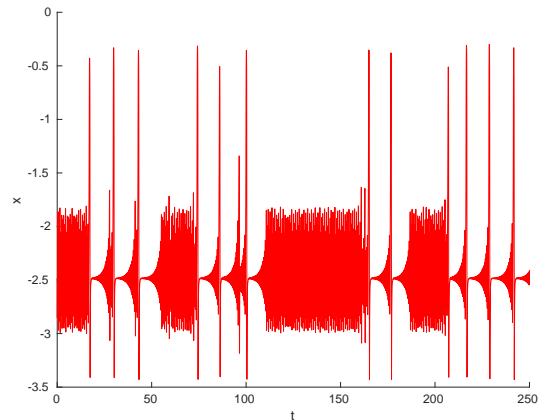


FIG. 6. Time series for the x coordinate of the model with the parameter a modified to be stochastic. With discrete time steps of approximately one day, $a = 7.3939 + 0.001 * N$ where N is a sample path of the normal distribution.

one another is concentrated in small regions of the state space of the model. If more detailed ENSO models behave similarly, this finding of bistability implies strong limits to the longer-term predictability of strong El Niño events. This needs to be considered when developing strategies for improving ENSO forecasts.

METHODS

Numerical simulations of the models in this paper were performed using an implementation of the algorithm DOP853 [24] in MATLAB. Stringent error tolerances (typically 10^{-12}) were used for calculating trajec-

tories and events (intersections of a trajectory with a specified cross-section).

The parameters used in this study were located in the following manner. The program MATCONT [25] was used to locate points of Hopf bifurcation and then to identify points of “generalized Hopf” bifurcations where the bifurcation is neither subcritical nor supercritical. Starting at parameters with a supercritical Hopf bifurcation and varying δ , periodic orbits were continued until they bifurcated through a period doubling cascade into a chaotic attractor. Further increases in δ led to a regime with an MMO attractor. Decreasing δ showed that the ranges of δ with MMO and chaotic attractors overlapped. The value of δ used in this study is in the overlap region.

The red and green markers in Figure (3) were obtained by computing intersections of trajectories in the two attractors with the cross-section $x = -2.874$. (This is the value of x at the equilibrium of the system.) A quadratic function $y = q(z)$ was fit with least squares (MATLAB command polyfit) to the intersection points of the chaotic attractor and the cross-section. The graph of this quadratic function was translated in the y direction to produce a 500x500 grid of initial conditions used in producing the figure. At each point in the grid, a trajectory was computed and then the point was colored with a value corresponding to the maximum value of y in its intersections with the cross-section. When the trajectory approaches the MMO, this maximum comes from the strong El Niño events and is larger than the values obtained from the chaotic attractor.

The strip of initial conditions used in computing Figure (4) was found by integrating initial conditions in the cross-section with $y = -0.4$ backward to their third return to the cross-section, fitting these points by a cubic curve and then translating this curve in the y direction. The third return to the cross-section was computed on a 100x100 grid in this region. The figure plots the value of y at the endpoint as a function of the initial point. The use of the third return in these calculations was motivated by the computation of an unstable periodic orbit in this region which intersects the cross-section three times.

Acknowledgments: The research of John Guckenheimer was partially supported by NSF Grant 1006272. Henk Dijkstra’s work was partially supported by a Mary Shepard B. Upson Visiting Professor position at the College of Engineering of Cornell University, Ithaca, NY. He thanks for Prof. Paul Steen (Cornell University) for being his host and the many interesting discussions. Axel Timmermann was supported by NOAA grant NA15OAR4310117.

-
- * jmg16@cornell.edu
- [1] M. J. McPhaden, A. Timmermann, M. J. Widlansky, M. A. Balmaseda, and T. N. Stockdale, *Bull. Amer. Meteor. Soc.* **96**, 1647 (2015).
 - [2] A. Federov, S. Harper, S. Philander, B. Winter, and A. Wittenberg, *Bull. Amer. Meteor. Soc.* **84**, 911 (2003).
 - [3] E. Tziperman, L. Stone, M. A. Cane, and H. Jarosh, *Science* **264**, 72 (1994).
 - [4] F.-F. Jin, J. Neelin, and M. Ghil, *Science* **264**, 70 (1994).
 - [5] T. Lian, D. Chen, Y. Tang, and Q. Wu, *Geophys. Res. Lett.* **41**, 3522 (2014).
 - [6] M. Roulston and J. Neelin, *Geophys. Res. Lett.* **27**, 3723 (2000).
 - [7] I. Eisenman, L. Yu, and E. Tziperman, *J. Climate* **18**, 5224 (2005).
 - [8] P. Webster and S. Yang, *Q. J. R. Meteor. Soc.* **118**, 877926 (1992).
 - [9] P. J. Webster, *Meteor. Atmos. Phys.* **56**, 33 (1995).
 - [10] M. Latif, T. P. Barnett, M. A. Cane, M. Flügel, N. E. Graham, H. von Storch, J.-S. Xu, and S. E. Zebiak, *Clim. Dynam.* **9**, 167 (1994).
 - [11] M. Mu, H. Xu, and W. Duan, *Geophys. Res. Lett.* **34**, L03709 (2007).
 - [12] W. Duan, X. Liu, K. Zhu, and M. Mu, *J. Geophys. Res.* **114**, C04022 (2009).
 - [13] Y. Yu, M. Mu, and W. Duan, *J. Climate* **25**, 1263 (2012).
 - [14] M. Suarez and P. Schopf, *J. Atmos. Sci.* **45**, 3283 (1988).
 - [15] E. Tziperman, M. Cane, S. Zebiak, Y. Xue, and B. Blumenthal, *J. Climate* **11**, 2191 (1998), ISSN 0894-8755.
 - [16] F. Jin, *J. Atmos. Sci.* **54**, 811 (1997), ISSN 0022-4928.
 - [17] A. Timmermann, F.-F. Jin, and J. Abshagen, *J. Atmos. Sci.* **60**, 152 (2003).
 - [18] A. Timmermann, H. U. Voss, and R. Pasmanter, *J. Physical Oceanography* **31**, 1579 (2001), [http://dx.doi.org/10.1175/1520-0485\(2001\)031<1579:EDSMOE>2.0.CO;2](http://dx.doi.org/10.1175/1520-0485(2001)031<1579:EDSMOE>2.0.CO;2), URL [http://dx.doi.org/10.1175/1520-0485\(2001\)031<1579:EDSMOE>2.0.CO;2](http://dx.doi.org/10.1175/1520-0485(2001)031<1579:EDSMOE>2.0.CO;2).
 - [19] A. Roberts, J. Guckenheimer, E. Widiasih, A. Timmermann, and C. K. R. T. Jones, *J. Atmos. Sci.* **73**, 1755 (2016), <http://dx.doi.org/10.1175/JAS-D-15-0191.1>, URL <http://dx.doi.org/10.1175/JAS-D-15-0191.1>.
 - [20] K. Stein, A. Timmermann, N. Schneider, F.-F. Jin, and M. F. Stuecker, *J. Climate* **27**, 5285 (2014), ISSN 0894-8755.
 - [21] C. Grebogi, E. Ott, and J. A. Yorke, *Science* **238**, 632 (1987), ISSN 0036-8075, URL <http://dx.doi.org/10.1126/science.238.4827.632>.
 - [22] K. Cobb, C. D. Charles, H. Cheng, and R. L. Edwards, *Nature* **424**, 271 (2003).
 - [23] S. McGregor, A. Timmermann, M. H. England, O. E. Timm, and A. T. Wittenberg, *Climate of the Past* **9**, 2269 (2013), ISSN 1814-9324.
 - [24] E. Hairer, S. P. Nørsett, and G. Wanner, *Solving ordinary differential equations. I*, vol. 8 of *Springer Series in Computational Mathematics* (Springer-Verlag, Berlin, 1993), 2nd ed., ISBN 3-540-56670-8, nonstiff problems.
 - [25] A. Dhooze, W. Govaerts, and Y. A. Kuznetsov, *ACM Trans. Math. Software* **29**, 141 (2003), ISSN 0098-3500, URL <http://dx.doi.org/10.1145/779359.779362>.